CHEMICAL ANALYSIS OF ASYMPTOTIC GIANT BRANCH STARS IN M62[*]

E. LAPENNA[1,2], A. MUCCIARELLI[1], F. R. FERRARO[1], L. ORIGLIA[2], B. LANZONI[1], D. MASSARI[2,3], AND E. DALESSANDRO[1]

[1] Dipartimento di Fisica e Astronomia, Università degli Studi di Bologna, Viale Berti Pichat 6/2, I-40127 Bologna, Italy
[2] INAF-Osservatorio Astronomico di Bologna, Via Ranzani, 1, I-40127 Bologna, Italy
[3] Kapteyn Astronomical Institute, University of Groningen, Landleven 12, 9747 AD Groningen, The Netherlands

ABSTRACT

We have collected UVES-FLAMES high-resolution spectra for a sample of 6 asymptotic giant branch (AGB) and 13 red giant branch (RGB) stars in the Galactic globular cluster (GC) M62 (NGC 6266). Here we present the detailed abundance analysis of iron, titanium, and light elements (O, Na, Mg, and Al). For the majority (five out of six) of the AGB targets, we find that the abundances of both iron and titanium determined from neutral lines are significantly underestimated with respect to those obtained from ionized features, the latter being, instead, in agreement with those measured for the RGB targets. This is similar to recent findings in other clusters and may suggest the presence of nonlocal thermodynamic equilibrium (NLTE) effects. In the O–Na, Al–Mg, and Na–Al planes, the RGB stars show the typical correlations observed for GC stars. Instead, all the AGB targets are clumped in the regions where first-generation stars are expected to lie, similar to what was recently found for the AGB population of NGC 6752. While the sodium and aluminum abundances could be underestimated as a consequence of the NLTE bias affecting iron and titanium, the oxygen line used does not suffer from the same effects, and the lack of O-poor AGB stars therefore is a solid result. We can thus conclude that none of the investigated AGB stars belongs to the second stellar generation of M62. We also find an RGB star with extremely high sodium abundance ([Na/Fe] = +1.08 dex).

Key words: globular clusters: individual (M62) – stars: abundances – stars: AGB and post-AGB – stars: late-type – techniques: spectroscopic

Supporting material: machine-readable table

1. INTRODUCTION

For stars with initial masses lower than $8\,M_{\odot}$, the asymptotic giant branch (AGB) is the last evolutionary stage characterized by thermonuclear reactions (in two shells surrounding an inert carbon–oxygen nucleus). The extended and cool atmospheres of AGB stars are ideal environments for the formation of dust grains and molecules. Moreover, the strong stellar winds developing during this phase return to the interstellar medium most of the material processed during the star life, thus playing a crucial role in the chemical evolution of the universe. These stars could also be at the origin of the self-enrichment processes that occurred in the early stages of globular cluster (GC) evolution, polluting the gas with the ejecta of high-temperature CNO-burning products (D'Ercole et al. 2008) and thus producing the observed chemical anomalies in light elements and the well-established Na–O and Mg–Al anticorrelations (see, e.g., Carretta et al. 2009b, 2009c; Mucciarelli et al. 2009; Gratton et al. 2012).

In spite of their importance and although the high luminosities of these stars can dominate the integrated light of a stellar population (e.g., Renzini & Buzzoni 1986; Ferraro et al. 1995; Hoefner et al. 1998; van Loon et al. 1999; Cioni & Habing 2003; Maraston 2005; Mucciarelli et al. 2006), only a few works have been dedicated to the detailed study of their chemical patterns, especially in GCs where the attention has been focused in particular on CN (Mallia 1978; Norris

et al. 1981; Briley et al. 1993), iron (Ivans et al. 1999, 2001; Lapenna et al. 2014; Mucciarelli et al. 2015a), sodium (Campbell et al. 2013; Johnson et al. 2014), and proton-capture elements (Worley et al. 2009). One of the first systematic chemical analyses of AGB stars in GCs was performed in M5 by Ivans et al. (2001), who found a significant discrepancy between the iron abundance derived from neutral and from single-ionized lines, in the sense of systematically lower values of [Fe I/H] with respect to [Fe II/H]. Very similar results, with differences up to ∼0.2 dex, have been recently found in a sample of AGB stars in 47 Tucanae (47Tuc) and NGC 3201 (Lapenna et al. 2014; Mucciarelli et al. 2015a, respectively). In all cases, the discrepancy cannot be explained by measurement uncertainties or an incorrect derivation of the atmospheric parameters, and it is not observed in red giant branch (RGB) stars belonging to the same cluster and analyzed in a homogeneous way. A proposed explanation is that AGB stars suffer from departures from local thermodynamic equilibrium (LTE) conditions, driven by iron overionization, in their atmospheres. In fact, this is expected to mainly affect (weaken) the neutral lines, while leaving unaltered the ionized features of the same chemical species (see Mashonkina et al. 2011). Following Thévenin & Idiart (1999), important nonlocal thermodynamic equilibrium (NLTE) effects are indeed expected in metal-poor stars with low values of gravity, mainly comparable to those typically observed near the RGB tip of GCs, and they should decrease with increasing metallicity. However, most of the giants studied by Ivans et al. (2001), Lapenna et al. (2014), and Mucciarelli et al. (2015a) are much fainter than the RGB tip, and 47Tuc is one of the most metal-rich GCs ([Fe/H] ∼ −0.8; Lapenna et al. 2014). Moreover, the available NLTE corrections are essentially the

same for stars with similar atmospheric parameters and cannot therefore explain why such a discrepancy is observed for AGB stars only and not even in all of them. Indeed, more recent results obtained in the metal-poor GC M22 show that also some RGB stars have Fe I abundances significantly lower than those determined from ionized lines (Mucciarelli et al. 2015b), thus adding further complexity to this puzzling situation.

In order to help understand the origin and the magnitude of these effects, detailed chemical analyses of giant stars in GCs with different metallicities and different properties are crucial. In this work we discuss the case of M62, for which we recently obtained high-resolution spectra for a sample of 19 RGB and AGB stars. This cluster is the tenth most luminous Galactic GC ($M_V = -9.18$, Harris 1996, 2010 edition), located near the Galactic bulge and affected by high and differential reddening, with an average color excess of $E(B - V) = 0.47$ mag (Harris 1996). It shows an extended horizontal branch (HB) and hosts a large population of millisecond pulsars and X-ray binaries and several blue straggler stars (D'Amico et al. 2001; Pooley et al. 2003; Beccari et al. 2006). However, in spite of its noticeable properties, only one study on its chemical composition by means of high-resolution spectra has been performed to date (Yong et al. 2014), and it is based on seven giant stars.

The paper is structured as follows. In Section 2 we describe the observations and the spectral analysis performed. In Section 3 we present the results obtained for the iron, titanium, and light-element abundances. Section 4 is devoted to the discussion and conclusions of the work.

2. OBSERVATIONS AND SPECTRAL ANALYSIS

We have observed a sample of 19 giant stars in the GC M62 by using the UVES-FLAMES@VLT spectrograph (Pasquini et al. 2000) within the Large Program 193.D-0232 (PI: Ferraro). The spectra have been acquired by using the grating 580 Red Arm CD#3, which provides a high spectral resolution ($R \sim 40{,}000$) and a spectral coverage between 4800 and 6800 Å. The 19 targets have been sampled by means of four different fiber configurations, in five pointings of 30 minutes each (one configuration has been repeated twice), during the nights of 2014 April 16 and June 2, 3, and 19. In each configuration, one or two fibers have been used to sample the sky for background-subtraction purposes. After careful visual inspection, only the (19) spectra with a signal-to-noise ratio larger than 50 have been kept in the analysis. The spectra have been reduced by using the dedicated ESO pipeline[4] performing bias subtraction, flat fielding, wavelength calibration, spectral extraction, and order merging. The sky background has been subtracted from each individual spectrum.

The target stars have been selected from the photometric catalog of Beccari et al. (2006), obtained from *HST* WFPC2 observations. Only stars brighter than $V = 15$ and sufficiently isolated (i.e., with no stellar sources of comparable or larger luminosity within a distance of 2″, and with no fainter stars within 1″) have been selected. Figure 1 shows the $(V, U - V)$ color–magnitude diagram (CMD) corrected for differential reddening following the procedure described in Massari et al. (2012) and adopting the extinction law by McCall (2004). The final sample includes six AGB and 13 RGB stars. All of the target stars are located within $\sim$85″ from the cluster center.

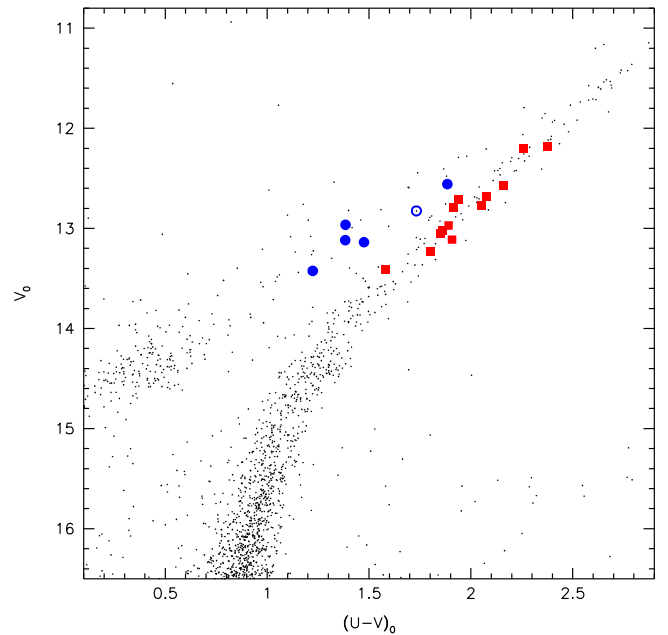[4] http://www.eso.org/sci/software/pipelines/

Figure 1. Reddening-corrected color–magnitude diagram of M62, with the targets of the present study highlighted: 13 RGB stars (red squares) and six AGB objects (blue circles). The empty circle marks AGB star 96.

Their identification number, coordinates, and magnitudes are listed in Table 1.

2.1. Radial Velocities

The radial velocities of our targets have been obtained by using the code DAOSPEC (Stetson & Pancino 2008) and by measuring the position of over 300 metallic lines distributed along the whole spectral range covered by the 580 Red Arm of UVES-FLAMES. The uncertainties have been computed as the dispersion of the velocities measured from each line divided by the square root of the number of lines used, and they turned out to be smaller than 0.05 km s^{-1}. Finally, we applied the heliocentric corrections computed with the IRAF task RVCORRECT. For each spectrum, the zero point of the wavelength calibration has been accurately checked by means of a few emission lines of the sky. The final velocities are listed in Table 1. They range from -109.8 to -53.4 km s^{-1}, with a mean value of -76.7 ± 3.6 km s^{-1} and a dispersion $\sigma = 15.6$ km s^{-1}. These values are in good agreement with the derivations of Dubath et al. (1997, $v_r = -71.8 \pm 1.6$ km s^{-1}, $\sigma = 16.0$ km s^{-1}) and Yong et al. (2014, $v_r = -70.1 \pm 1.4$ km s^{-1}, $\sigma = 14.3$ km s^{-1}), the small differences being likely due to the small statistics.

The most discrepant target (id = 79), with a radial velocity of -109.85 km s^{-1}, is still within 2σ from the systemic velocity of the cluster. By using the Besançon Galactic model (Robin et al. 2003), we extracted a sample of about 5,300 field stars in the direction of M62, finding a quite broad and asymmetric radial velocity distribution, with mean $v_r \simeq -60$ km s^{-1} and dispersion $\sigma = 80$ km s^{-1}, which partially overlaps that of the cluster. On the other hand, only a few percent of the stars studied in that region close to the Galactic bulge have a [Fe/H] < -1.0 dex (see, e.g., Zoccali et al. 2008; Hill et al. 2011; Johnson et al. 2013; Ness et al. 2013). Thus, taking into account the metallicity of star 79 (see below), its position in the CMD, and its distance from the cluster center ($d \sim 38{.}^{\prime\prime}5$), we

Table 1
Photometric Properties and Radial Velocities of the RGB and AGB Samples

ID	R.A. (J2000)	decl. (J2000)	U (mag)	V (mag)	U_0 (mag)	V_0 (mag)	RV (km s^{-1})	Type
50	255.2961736	−30.1122536	17.458	14.061	14.558	12.184	−95.41 ± 0.06	R
54	255.2968276	−30.1110148	17.465	14.149	14.462	12.206	−68.41 ± 0.04	R
76	255.3016326	−30.0879873	17.578	14.416	14.734	12.576	−69.34 ± 0.06	R
82	255.2908040	−30.1230200	17.378	14.478	14.649	12.712	−56.67 ± 0.04	R
89	255.3053120	−30.1235390	17.694	14.584	14.759	12.685	−68.78 ± 0.04	R
95	255.2683150	−30.1061800	17.689	14.624	14.821	12.768	−85.92 ± 0.06	R
97	255.2746210	−30.1078150	17.551	14.632	14.703	12.789	−92.22 ± 0.06	R
104	255.2990264	−30.1195799	17.502	14.680	14.861	12.971	−81.19 ± 0.04	R
118	255.2953240	−30.1054710	17.584	14.771	14.883	13.023	−90.41 ± 0.06	R
127	255.3064600	−30.0967810	17.775	14.895	15.020	13.112	−55.24 ± 0.06	R
133	255.3025803	−30.1265560	17.819	14.939	14.903	13.052	−90.70 ± 0.05	R
145	255.2959190	−30.1263240	17.831	15.041	15.031	13.229	−63.56 ± 0.05	R
157	255.2998135	−30.0934941	17.720	15.174	14.988	13.406	−74.04 ± 0.05	R
79	255.3060883	−30.1031433	17.335	14.430	14.443	12.558	−109.85 ± 0.06	A
96	255.2885360	−30.1173880	17.345	14.629	14.558	12.826	−81.49 ± 0.07	A
116	255.2778880	−30.1205350	17.130	14.764	14.348	12.963	−87.57 ± 0.09	A
128	255.2980470	−30.1078870	17.248	14.895	14.501	13.117	−72.72 ± 0.08	A
135	255.2914560	−30.1287900	17.416	14.952	14.613	13.138	−60.08 ± 0.07	A
158	255.3017290	−30.1013070	17.361	15.180	14.647	13.424	−53.49 ± 0.07	A

Note. Identification number, coordinates, U, V, U_0, and V_0 magnitudes, heliocentric radial velocity, and type of star (R = RGB, A = AGB).

conclude that it is likely a genuine cluster member, and we therefore keep it in the following analysis.

2.2. Atmospheric Parameters and Stellar Masses

First-guess effective temperature (T_{eff}) and surface gravity ($\log g$) values for each target have been derived by using the photometric information. Temperatures have been estimated by using the $(U − V)_0 − T_{eff}$ calibration of Alonso et al. (1999). Gravities have been computed with the Stefan–Boltzmann equation by adopting the color excess quoted above, a distance modulus $(m − M)_0 = 14.16$ mag (Harris 1996), and the bolometric correction from Alonso et al. (1999). For the RGB stars, we adopted a mass of $0.82 M_\odot$, according to the best-fit isochrone retrieved from the PARSEC data set (Bressan et al. 2012), and computed for an age of 12 Gyr and a metallicity Z = 0.0013. For the AGB stars, we adopted a mass of $0.61 M_\odot$, according to the median value of the HB mass range estimated by Gratton et al. (2010).

Then we performed a spectroscopic analysis as done in Lapenna et al. (2014) and Mucciarelli et al. (2015a), constraining the atmospheric parameters as follows: (1) spectroscopic temperatures have been obtained by requiring that no trend exists between iron abundance and excitation potential, (2) the gravity was derived by using the Stefan–Boltzmann equation with the value of T_{eff} thus obtained, and (3) the microturbulent velocity was determined by requiring that no trend exists between iron abundance and line strength. In order to evaluate the effects of a different procedure in the derivation of the atmospheric parameters and abundances, we have also performed a spectroscopic determination of the surface gravities by modifying condition (2) and imposing that the same abundance is obtained from neutral and single-ionized iron lines (ionization balance).

Table 2
Wavelength, Element, Oscillator Strength, Excitation Potential, and Reference Source of Adopted Lines

Wavelength (Å)	El.	log gf	E.P. (eV)	References
4962.572	Fe I	−1.182	4.178	Fuhr & Wiese (2006)
4967.897	Fe I	−0.534	4.191	K
4969.917	Fe I	−0.710	4.217	Fuhr et al. (1988)
4982.499	Fe I	0.164	4.103	K
4983.250	Fe I	−0.111	4.154	K
4985.547	Fe I	−1.331	2.865	Fuhr & Wiese (2006)
4950.106	Fe I	−1.670	3.417	Fuhr et al. (1988)
4962.572	Fe I	−1.182	4.178	Fuhr & Wiese (2006)
4967.897	Fe I	−0.534	4.191	K
4969.917	Fe I	−0.710	4.217	Fuhr et al. (1988)

Note. K = Oscillator strengths (OS) from the R. L. Kurucz online database of observed and predicted atomic transitions (see http://kurucz.harvard.edu), NIST = OS from NIST database (see http://www.nist.gov/pml/data/asd.cfm), S = OS from solar analysis by F. Castelli (see http://wwwuser.oats.inaf.it/castelli/linelists.html). For the Al I lines we derived astrophysical oscillator strengths (labeled as S*) by using the solar flux spectra of Neckel & Labs (1984) and the model atmosphere for the Sun computed by F. Castelli (http://wwwuser.oats.inaf.it/castelli/sun/ap00t5777g44377k1odfnew.dat) adopting the solar abundances of Grevesse & Sauval (1998). The other atomic data have been taken from Wolnik & Berthel 1973, Martin et al. 1988, O'Brian et al. 1991, Storey & Zeippen 2000, Raassen & Uylings 1998, Lawler et al. 2013, and Wood et al. 2013.

(This table is available in its entirety in machine-readable form.)

2.3. Chemical Abundances

The chemical abundances of Fe, Ti, Na, Mg, and Al have been derived with the package GALA[5] (Mucciarelli et al.

---

5   http://www.cosmic-lab.eu/gala/gala.php

Table 3
Atmospheric Parameters and Iron and Titanium Abundances of the Measured RGB and AGB Stars

ID	$T_{\rm eff}$ (K)	log g (dex)	$v_{\rm turb}$ (km s^{-1})	[Fe I/H] (dex)	$n_{\rm Fe\,I}$	[Fe II/H] (dex)	$n_{\rm Fe\,II}$	[Ti I/H] (dex)	$n_{\rm Ti\,I}$	[Ti II/H] (dex)	$n_{\rm Ti\,II}$
50	4225	0.85	1.30	-1.13 ± 0.01	128	-1.13 ± 0.02	12	-0.91 ± 0.01	58	-0.95 ± 0.05	12
54	4215	0.85	1.40	-1.17 ± 0.01	130	-1.14 ± 0.01	7	-0.99 ± 0.01	63	-1.06 ± 0.03	14
76	4375	1.15	1.35	-1.05 ± 0.01	106	-1.00 ± 0.03	7	-0.87 ± 0.02	37	-0.88 ± 0.05	6
82	4295	1.15	1.30	-1.06 ± 0.01	104	-1.02 ± 0.03	11	-0.89 ± 0.01	45	-0.92 ± 0.06	7
89	4355	1.15	1.50	-1.07 ± 0.01	127	-1.08 ± 0.03	10	-0.78 ± 0.01	62	-0.93 ± 0.03	14
95	4365	1.20	1.45	-1.07 ± 0.01	134	-1.10 ± 0.02	11	-0.89 ± 0.01	58	-0.93 ± 0.04	15
97	4425	1.25	1.40	-1.01 ± 0.01	142	-1.02 ± 0.02	12	-0.82 ± 0.01	50	-0.96 ± 0.05	14
104	4325	1.20	1.30	-1.11 ± 0.01	108	-1.00 ± 0.03	7	-0.94 ± 0.01	40	-0.90 ± 0.05	7
118	4450	1.35	1.40	-1.05 ± 0.01	140	-1.03 ± 0.01	8	-0.81 ± 0.01	56	-0.88 ± 0.03	13
127	4425	1.35	1.35	-1.06 ± 0.01	102	-0.95 ± 0.02	10	-0.90 ± 0.02	57	-0.90 ± 0.05	15
133	4450	1.35	1.40	-1.10 ± 0.01	142	-1.05 ± 0.01	9	-0.89 ± 0.01	57	-0.91 ± 0.04	15
145	4475	1.45	1.30	-1.06 ± 0.01	146	-0.98 ± 0.02	10	-0.88 ± 0.01	47	-0.92 ± 0.04	13
157	4545	1.55	1.45	-1.04 ± 0.01	136	-1.01 ± 0.02	10	-0.83 ± 0.01	52	-0.84 ± 0.05	13
79	4415	1.00	1.55	-1.19 ± 0.01	131	-1.08 ± 0.01	8	-1.08 ± 0.01	48	-1.03 ± 0.04	15
96	4450	1.15	1.50	-1.10 ± 0.01	130	-1.13 ± 0.03	11	-0.71 ± 0.03	33	-0.88 ± 0.07	9
116	4760	1.35	1.80	-1.24 ± 0.01	134	-1.13 ± 0.03	9	-1.12 ± 0.02	27	-0.99 ± 0.04	13
128	4760	1.45	1.60	-1.21 ± 0.01	138	-1.10 ± 0.04	12	-1.11 ± 0.02	33	-0.95 ± 0.04	14
135	4635	1.40	1.55	-1.14 ± 0.01	128	-0.98 ± 0.03	10	-1.08 ± 0.02	33	-0.88 ± 0.04	13
158	4840	1.60	1.65	-1.19 ± 0.01	142	-1.01 ± 0.02	11	-1.10 ± 0.02	27	-0.92 ± 0.05	14

Note. Identification number, spectroscopic temperature and photometric gravities, microturbulent velocities, iron and titanium abundances with internal uncertainty and number of lines used, as measured from neutral and single-ionized lines. For all of the stars a global metallicity of [M/H] = −1.0 dex has been assumed for the model atmosphere. The adopted solar values are from Grevesse & Sauval (1998).

2013b), which adopts the classical method to derive the abundances from the measured EWs of metallic unblended lines. The EW and the error of each line were obtained using DAOSPEC, iteratively launched by means of the 4DAO[6] code (Mucciarelli 2013a). The lines considered in the analysis have been selected from suitable synthetic spectra at the UVES-FLAMES resolution and computed with the SYNTHE package (Sbordone 2005) by using the guess atmospheric parameters and the metallicity derived by Yong et al. (2014). The model atmospheres have been computed with the ATLAS9[7] code. We adopted the atomic and molecular data from the last release of the Kurucz/Castelli compilation[8] and selected only the lines predicted to be unblended. The selected lines and the atomic data adopted in the analysis are listed in Table 2.

As detailed in Table 3, we used 100–150 Fe I lines and 7–12 Fe II lines to derive the iron abundances, and 25–60 lines of Ti I and 6–15 lines of Ti II to derive the abundances of titanium. For Na I, Mg I, and Al I, only few lines are available, namely those at 5682–5688 and 6154–6160 Å for Na I, the line at 5711 Å and the doublet at 6318–6319 Å for Mg I, and the doublet at 6696–6698 Å for Al I. The O abundances have been derived from spectral synthesis in order to take into account the blending between the forbidden [O I] line at 6300.3 Å and a Ni transition. For Ni we adopted the average abundance obtained by Yong et al. (2014), while for stars located in the upper RGB we assumed average C and N abundances according to Gratton et al. (2000), all rescaled to the assumed solar reference values (Grevesse & Sauval 1998). Because in some spectra the [O I] line was also partially blended with a telluric line, the spectra have been cleaned by using suitable synthetic spectra obtained

with the TAPAS tool (Bertaux et al. 2014). For some stars, the [O I] line is not detectable, so only upper limits are obtained. As solar reference abundances we adopted the Caffau et al. (2011) value for O, and those of Grevesse & Sauval (1998) for all of the other elements.

For the computation of the global uncertainties on the final abundances, we took into account two main sources of errors, which have been added in quadrature.

1. The error arising from the EW measurements. For each star we computed this term by dividing the line-to-line dispersion by the square root of the number of lines used. Thanks to the high quality of the spectra and to the number of lines that can be exploited, this term turned out to be very small, especially for Fe I and Ti I (providing up to 150 lines). For these species, the line-to-line scatter is smaller than 0.1 dex, leading to internal uncertainties lower than 0.01–0.02 dex. For Fe II and Ti II, the number of lines ranges from seven up to 15, leading to an uncertainty of about 0.02–0.03 dex. For the other chemical species, the number of measured lines is much smaller (1–4). Hence, the average uncertainties are of the order of 0.06–0.08 dex for O I, Na I, Mg I, and Al I.

2. The error arising from atmospheric parameters. For the computation of this term, we varied each parameter by the 1σ error obtained from the previous analysis. We have found that representative errors for $T_{\rm eff}$, log g, and $v_{\rm turb}$ are ∼50 K, 0.1 dex, and 0.1 km s^{-1}, respectively, for both the RGB and the AGB samples. Thus we decided to adopt these values as the 1σ error for all stars. We also checked the effect of a ±0.1 dex change in the metallicity of the model atmosphere, finding variations smaller than ±0.01 dex on the final abundances.

---

[6] http://www.cosmic-lab.eu/4dao/4dao.php
[7] http://wwwuser.oats.inaf.it/castelli/sources/atlas9codes.html
[8] http://wwwuser.oats.inaf.it/castelli/linelists.html

Table 4
O I, Na I, Mg I, Al I, Ti I, and Ti II Abundances of the RGB and AGB Samples

ID	[O I/Fe II] (dex)	[Na I/Fe I]$_{LTE}$ (dex)	[Na I/Fe I]$_{NLTE}$ (dex)	n_{Na}	[Mg I/Fe I] (dex)	n_{Mg}	[Al I/Fe I] (dex)	n_{Al}	[Ti I/Fe I] (dex)	$n_{Ti I}$	[Ti II/Fe II] (dex)	$n_{Ti II}$
50	0.39 ± 0.05	−0.01 ± 0.12	0.11 ± 0.09	4	0.47 ± 0.03	3	0.28 ± 0.01	2	0.22 ± 0.02	58	0.18 ± 0.05	12
54	0.35 ± 0.04	0.17 ± 0.10	0.30 ± 0.06	4	0.51 ± 0.02	3	0.28 ± 0.00	2	0.18 ± 0.01	63	0.08 ± 0.03	14
76	<−0.16	0.34 ± 0.11	0.42 ± 0.07	4	0.37 ± 0.02	3	0.66 ± 0.02	2	0.18 ± 0.02	37	0.12 ± 0.05	6
82	0.31 ± 0.07	−0.05 ± 0.08	0.05 ± 0.04	4	0.40 ± 0.03	3	0.20 ± 0.02	2	0.17 ± 0.02	45	0.09 ± 0.07	7
89	<−0.28	1.04 ± 0.06	1.08 ± 0.02	4	0.46 ± 0.02	3	0.78 ± 0.04	2	0.29 ± 0.02	62	0.15 ± 0.04	14
95	<−0.36	0.31 ± 0.17	0.40 ± 0.16	4	0.33 ± 0.05	3	1.19 ± 0.06	2	0.18 ± 0.02	58	0.17 ± 0.05	15
97	<−0.34	0.41 ± 0.14	0.47 ± 0.09	4	0.35 ± 0.06	2	1.08 ± 0.04	2	0.19 ± 0.02	50	0.06 ± 0.05	14
104	0.25 ± 0.08	0.01 ± 0.11	0.11 ± 0.07	4	0.43 ± 0.06	3	0.29 ± 0.05	1	0.17 ± 0.02	40	0.10 ± 0.06	7
118	0.39 ± 0.05	−0.03 ± 0.10	0.05 ± 0.07	4	0.40 ± 0.06	2	0.29 ± 0.03	2	0.24 ± 0.02	56	0.15 ± 0.03	13
127	0.05 ± 0.09	0.08 ± 0.11	0.17 ± 0.07	4	0.39 ± 0.02	3	0.44 ± 0.04	1	0.16 ± 0.02	57	0.05 ± 0.05	15
133	<−0.17	0.40 ± 0.10	0.46 ± 0.06	4	0.34 ± 0.05	2	1.12 ± 0.06	2	0.21 ± 0.01	57	0.14 ± 0.04	15
145	0.13 ± 0.07	−0.03 ± 0.08	0.05 ± 0.06	4	0.38 ± 0.01	3	0.19 ± 0.04	2	0.18 ± 0.01	47	0.07 ± 0.04	13
157	<−0.40	0.55 ± 0.10	0.59 ± 0.06	4	0.36 ± 0.02	3	0.96 ± 0.03	2	0.21 ± 0.01	52	0.17 ± 0.05	13
79	0.37 ± 0.05	−0.20 ± 0.06	−0.04 ± 0.04	4	0.58 ± 0.08	2	0.20 ± 0.07	1	0.11 ± 0.01	48	0.05 ± 0.04	15
96	0.35 ± 0.06	−0.03 ± 0.08	0.09 ± 0.04	4	0.43 ± 0.05	3	0.33 ± 0.06	1	0.39 ± 0.04	33	0.25 ± 0.08	9
116	0.17 ± 0.07	0.13 ± 0.04	0.23 ± 0.03	4	0.38 ± 0.04	2	0.46 ± 0.05	1	0.12 ± 0.02	27	0.14 ± 0.05	13
128	0.19 ± 0.06	−0.06 ± 0.10	0.04 ± 0.09	4	0.50 ± 0.09	3	0.44 ± 0.07	1	0.10 ± 0.03	33	0.15 ± 0.06	14
135	0.30 ± 0.07	−0.20 ± 0.04	−0.08 ± 0.03	4	0.47 ± 0.03	3	0.28 ± 0.07	1	0.06 ± 0.02	33	0.11 ± 0.05	13
158	0.19 ± 0.05	0.13 ± 0.06	0.20 ± 0.03	3	0.48 ± 0.08	3	0.46 ± 0.05	1	0.09 ± 0.02	27	0.09 ± 0.05	14

Note. The oxygen abundance has been derived from the 6300.3 Å [O I] line, and the abundances of sodium have been reported without and with NLTE corrections computed following Gratton et al. (1999). The reference solar values are taken from Caffau et al. (2011) for the oxygen and from Grevesse & Sauval (1998) for the other species.

3. RESULTS

The determination of abundances and abundance ratios of the various chemical elements is described below. The adopted atmospheric parameters and the measured iron and titanium abundances for the observed RGB and AGB stars are listed in Table 3, while the abundances of the light elements are listed in Table 4. In Table 5 we present the global abundance uncertainty of one RGB and one AGB star, as well as the uncertainties obtained by varying each atmospheric parameter independently. Since this approach does not take into account the correlations among different parameters, the global error can be slightly overestimated.

Since star 96 presents an anomalous behavior with respect to the other AGB targets, in the following analysis it is not included in the AGB sample (thus counting five stars), and it is discussed separately at the end of Section 3.1.

3.1. Iron and Titanium

By using spectroscopic gravities (thus imposing that the same iron abundance is obtained from neutral and from single-ionized lines), the average values measured for the RGB and the AGB subsamples are [Fe/H]$_{RGB}$ = −1.10 ± 0.01 (σ = 0.04 dex) and [Fe/H]$_{AGB}$ = −1.18 ± 0.01 (σ = 0.03 dex). These values are consistent (within 1–2 σ) with previous abundance determinations of M62 giants, whether they are on the RGB or on the AGB: [Fe/H] = −1.12 dex (Kraft & Ivans 2003),[9] [Fe/H] = −1.18 ± 0.07 dex (Carretta et al. 2009a), and [Fe/H] = −1.15 ± 0.02 dex (σ = 0.05 dex, Yong et al. 2014).

By using photometric gravities (and not imposing ionization balance), we determined the iron abundances separately from neutral and from single-ionized lines. For the 13 RGB stars we

---

[9] We refer to the average value computed with Kurucz models without overshooting; see Kraft & Ivans (2003) for details.

Table 5
Abundance Uncertainties due to the Atmospheric Parameters for the Stars 157 and 158

Species	Global Uncertainty (dex)	δT_{eff} ±50 K (dex)	$\delta \log g$ ±0.1 (dex)	δv_{turb} ±0.1 km s^{-1} (dex)
		157 (RGB)		
Fe I	±0.07	±0.04	±0.00	∓0.06
Fe II	±0.08	∓0.05	±0.05	∓0.04
O I	±0.04	±0.01	±0.03	∓0.02
Na I	±0.05	±0.04	∓0.01	∓0.02
Mg I	±0.04	±0.03	±0.00	∓0.03
Al I	±0.04	±0.04	±0.00	∓0.02
Ti I	±0.09	±0.08	±0.00	∓0.03
Ti II	±0.05	∓0.02	±0.04	∓0.03
		158 (AGB)		
Fe I	±0.07	±0.06	±0.00	∓0.04
Fe II	±0.07	∓0.03	±0.05	∓0.03
O I	±0.05	±0.02	±0.04	∓0.02
Na I	±0.04	±0.04	±0.00	∓0.01
Mg I	±0.03	±0.03	±0.00	∓0.01
Al I	±0.03	±0.03	±0.00	∓0.00
Ti I	±0.08	±0.08	±0.00	∓0.01
Ti II	±0.06	∓0.01	±0.05	∓0.03

Note. The second column shows the global uncertainty calculated by adding in quadrature the single uncertainties. The other columns list the uncertainties obtained by varying only one parameter at a time while keeping the others fixed.

obtained [Fe I/H]$_{RGB}$ = −1.07 ± 0.01 dex (σ = 0.04 dex) and [Fe II/H]$_{RGB}$ = −1.04 ± 0.02 dex (σ = 0.06 dex). For the five AGB stars we measured [Fe I/H]$_{AGB}$ = −1.19 ± 0.01 dex (σ = 0.04 dex) and [Fe II/H]$_{AGB}$ = −1.06 ± 0.02 dex (σ = 0.06 dex). The average difference between the values of
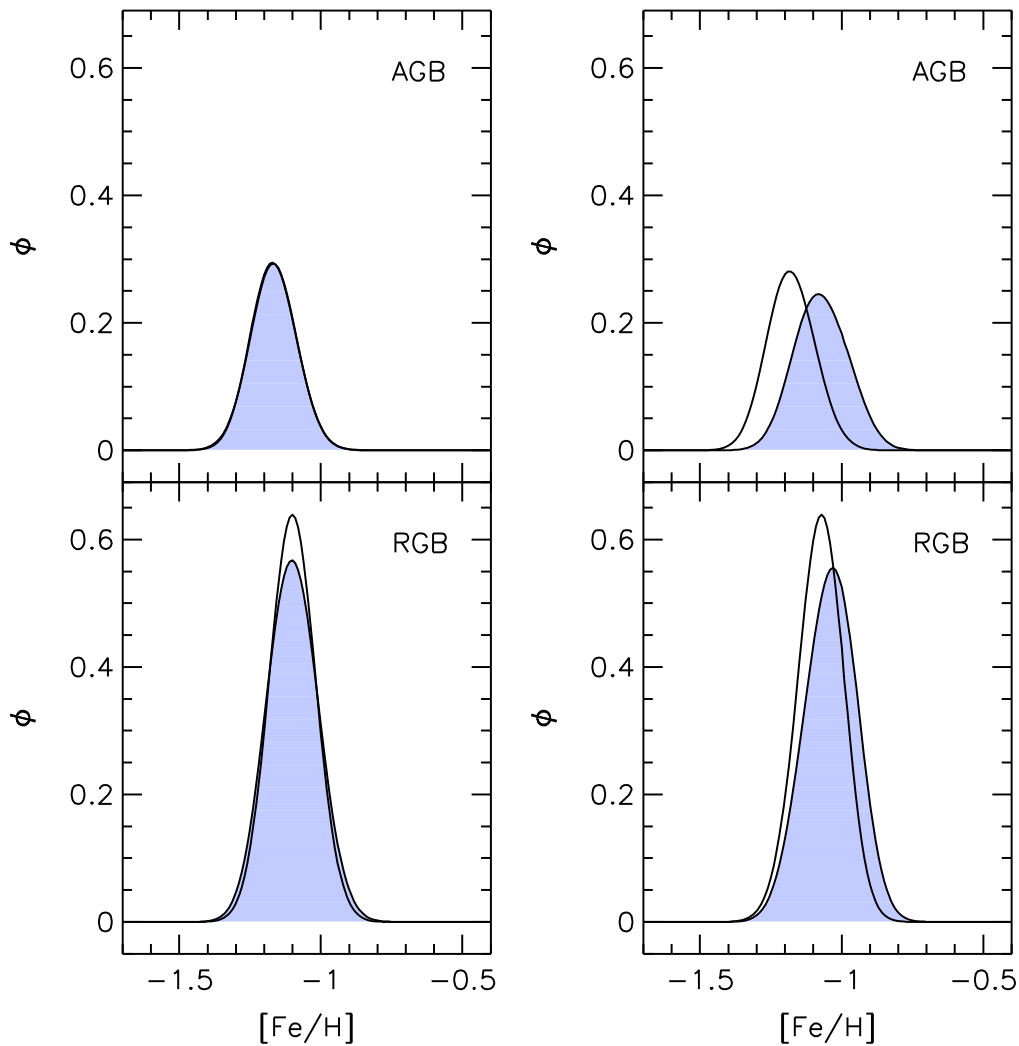
Figure 2. Left panels: generalized histograms for [Fe I/H] (empty histograms) and [Fe II/H] (blue shaded histograms) obtained by adopting spectroscopic gravities, for AGB stars (top panel) and the RGB sample (bottom panel). Right panels: as in the left panels, but for the iron abundances obtained by adopting photometric gravities.

log g derived spectroscopically and those derived photometrically are 0.09 dex (σ = 0.10 dex) and 0.30 dex (σ = 0.20 dex) for the RGB and the AGB samples, respectively. Figure 2 shows the generalized histograms of the iron abundances for the RGB and the AGB samples separately, obtained by using spectroscopic (left panels) and photometric gravities (right panels). By construction, the distributions of [Fe I/H] and [Fe II/H] essentially coincide if spectroscopic gravities are assumed. Instead, the two distributions significantly differ in the case of AGB stars if photometric gravities are adopted. In particular, the average iron abundances of RGB stars measured from neutral and single-ionized lines are consistent within the uncertainties, whereas a difference of −0.13 dex, exceeding 5σ, is found for the AGB sample. Moreover, RGB and AGB stars show very similar (well within 1σ) average values of [Fe II/H], whereas the neutral abundances of AGB stars are significantly lower (by 0.12 dex) than those of the RGB targets.

When using photometric gravities, similar results are obtained for titanium, the only other chemical species presenting a large number of neutral and single-ionized lines. For the RGB sample we find [Ti I/H]$_{\rm RGB}$ = −0.88 ± 0.01 dex (σ = 0.06 dex) and [Ti II/H]$_{\rm RGB}$ = −0.92 ± 0.01 dex

(σ = 0.05 dex). For the AGB stars we measure [Ti I/H]$_{\rm AGB}$ = −1.10 ± 0.01 dex (σ = 0.02 dex) and [Ti II/H]$_{\rm AGB}$ = −0.95 ± 0.02 dex (σ = 0.06 dex). In this case, the average abundance of AGB stars from neutral lines is lower than that of the RGB sample by 0.21 dex (whereas such a difference amounts to only 0.04 dex for the RGB sample). In Figure 3 we report the differences between the iron (top left panel) and the titanium (top right panel) abundances derived from neutral and from single-ionized lines, as a function of the abundances from the neutral species, obtained for each observed star assuming photometric gravities. Clearly, with the only exception of star 96 (plotted as an empty circle in the figure), the AGB and the RGB samples occupy distinct regions in these planes because of systematically lower values of the AGB abundances derived from the neutral species.

Such a difference can also be directly appreciated by visually inspecting the line strengths in the observed spectra and their synthetic best fits. As an example, in Figure 4 we show the observed spectra of an RGB and an AGB star around some Fe I and Fe II lines, together with synthetic spectra calculated with the appropriate atmospheric parameters and the metallicity derived from Fe II and from Fe I lines. As is apparent, the synthetic spectrum computed adopting the Fe II abundance well
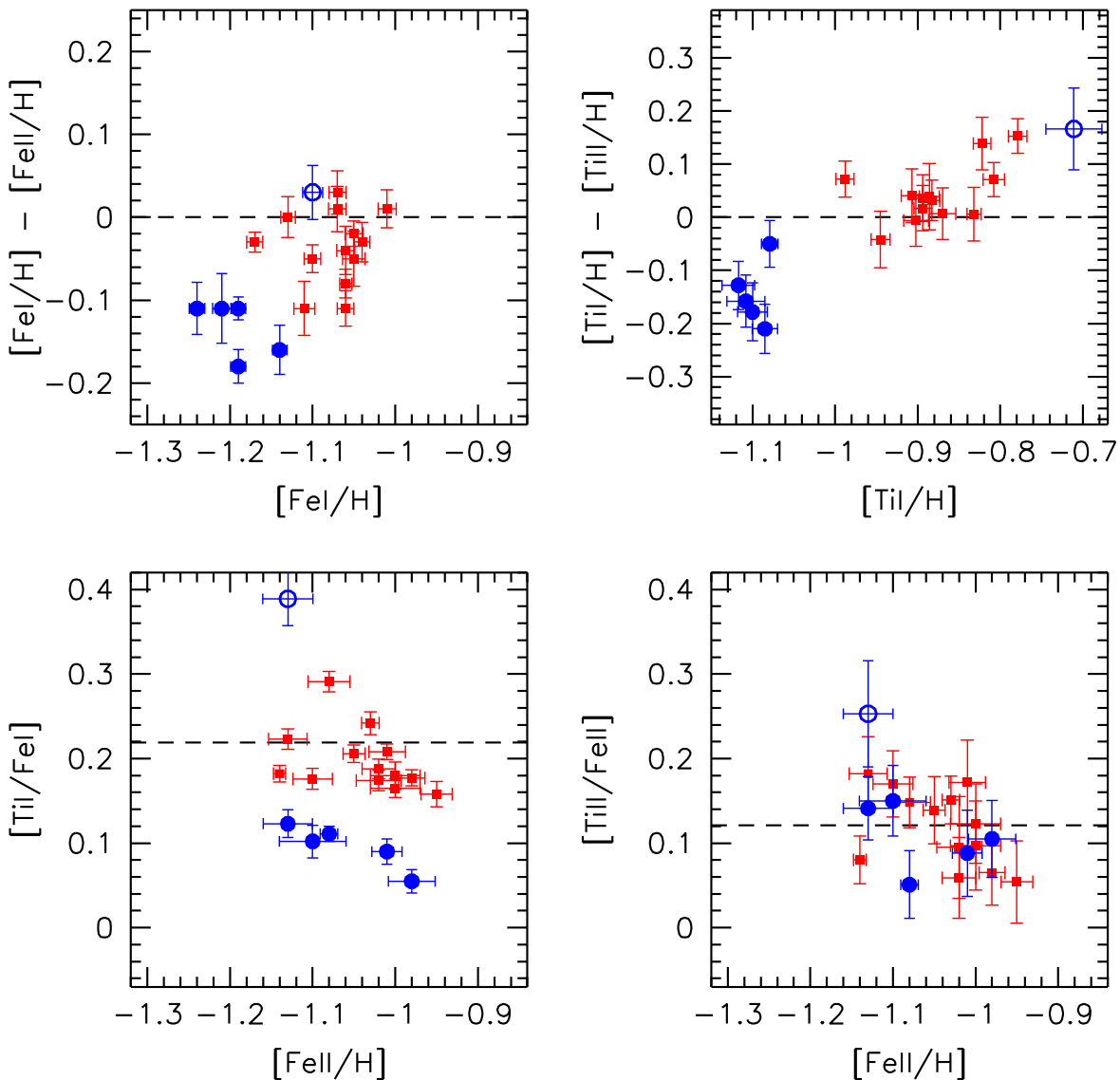
Figure 3. Top panels: difference between the chemical abundances derived from neutral and single-ionized lines, as a function of that obtained from neutral lines, for iron (left panel) and titanium (right panel). Symbols are as in Figure 1. Bottom panels: [Ti I/Fe I] and [Ti II/Fe II] abundance ratios as a function of [Fe II/H] for the studied samples.

reproduces all of the observed lines in the case of the RGB star, whereas it fails to fit the neutral features observed in the AGB target, independent of the excitation potential (thus guarantee-ing that the effect cannot be due to inadequacies in the adopted temperature). On the other hand, the abundance measured from Fe I lines is too low to properly reproduce the depth of the ionized features of the AGB star. This clearly demonstrates a different behavior of iron lines in AGB and RGB stars.

To investigate the origin of the discrepancy between Fe I and Fe II abundances obtained for the AGB sample, we checked the impact of the adopted stellar mass on the estimate of the photometric gravity. As described in Section 2.2, for the AGB stars we assumed a mass of $0.61\,M_\odot$, corresponding to the median value of the distribution obtained for HB stars by Gratton et al. (2010), ranging from 0.51 to $0.67\,M_\odot$. By adopting the lowest mass ($0.51\,M_\odot$), the average value of $\log g$

decreases by $\sim 0.08\,\text{dex}$, but when assuming the largest value, $\log g$ increases by $0.04\,\text{dex}$. Such small gravity variations[10] have a negligible impact on the abundances derived from the neutral iron lines, and the impact is still modest (at a level of a few hundredths of a dex) on the abundances derived from single-ionized lines. The only way to obtain (by construction) the same abundance from Fe I and Fe II lines is to use the spectroscopic values of $\log g$ derived from the ionization balance (Section 2.2). However, these gravities correspond to stellar masses in the range $0.25\text{–}0.3\,M_\odot$, which are totally unphysical for evolved stars in GCs.

A possible explanation of the observed discrepancy could be a departure from LTE conditions in the atmosphere of AGB stars. In fact, lines originated by atoms in the minority ionization state usually suffer from NLTE effects, while those originated by atoms in the dominant ionization state are unaffected (see, e.g., Mashonkina et al. 2011). Thus, if this is the case, the most reliable determination of the iron abundance is that provided by [Fe II/H] because the majority of iron atoms

---

[10] Note that the increase of $\log g$ is essentially the same (0.05 dex) even if the mass provided by the best-fit isochrone ($0.72\,M_\odot$) is adopted.
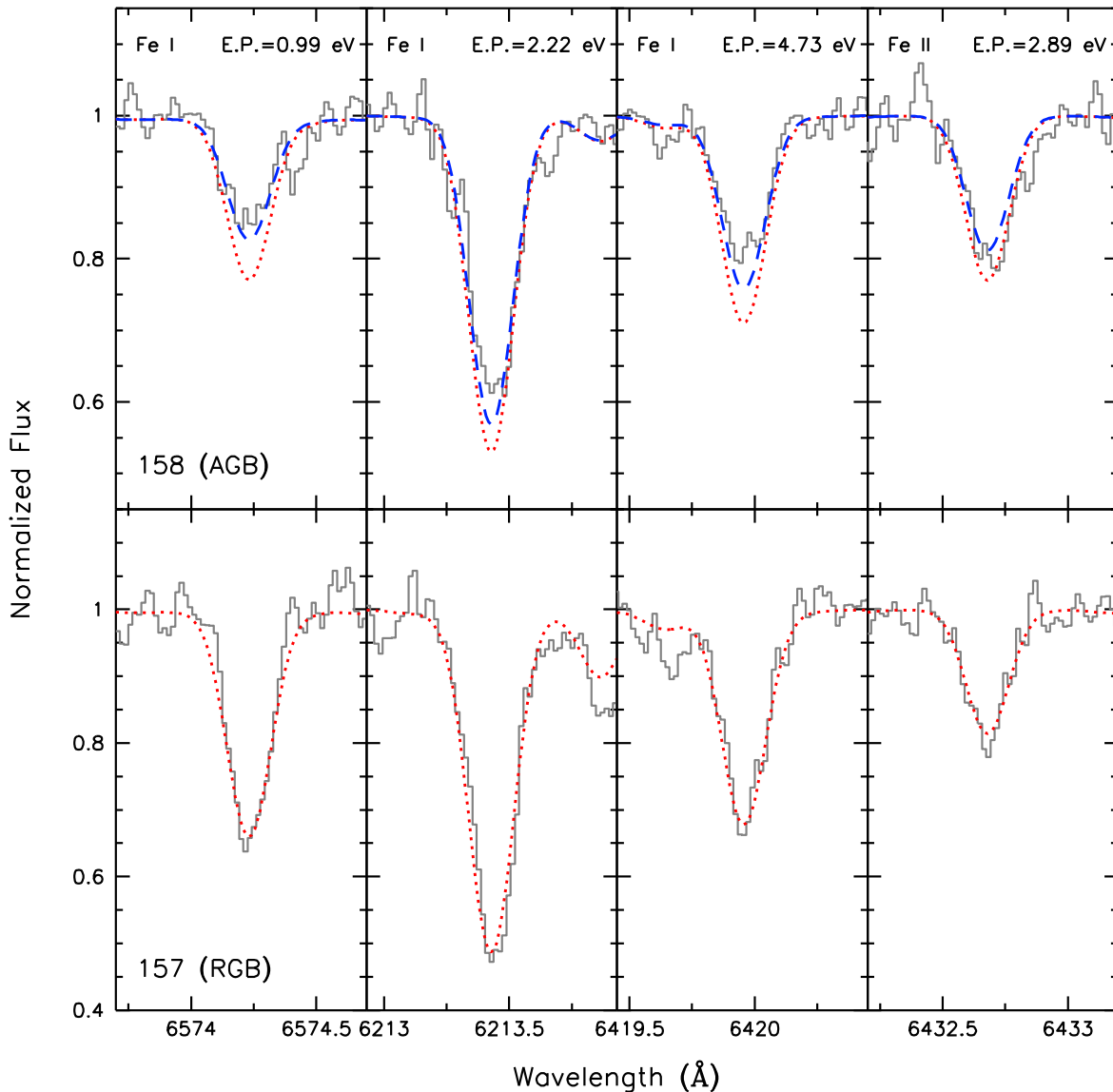
Figure 4. Comparison between observed and synthetic spectra for AGB star 158 (upper panels) and RGB star 15 (lower panels) around three Fe I lines with different excitation potentials and one Fe II line (see labels). The observed spectra are marked with gray lines. The synthetic spectra have been computed by using the measured [Fe I/H] (blue dashed line) and [Fe II/H] (red dotted lines) abundances. Since the two abundances are practically identical for the RGB star, only one synthetic spectrum is shown in the lower panels.

are in the first ionized state in giant stars. Moreover, following Ivans et al. (2001), the degree of overionization of the neutral species should be (at least at a first order) the same as the one affecting Fe I lines. Hence, the correct way to obtain a [X/Fe] abundance ratio is to compute it with respect to the Fe I abundance if [X/H] is derived from minority species, and with respect to Fe II if [X/H] is obtained from majority species. In the lower panels of Figure 3 we present the [Ti II/Fe II] and the [Ti I/Fe I] abundance ratios as a function of the iron abundance derived from single-ionized lines.

As expected, the abundances of AGB stars agree with those of the RGB sample when single-ionized (dominant state) titanium lines are used. For [Ti I/Fe I] a systematic offset of the AGB sample toward lower values is still observable (although reduced), thus indicating the possible presence of residual NLTE effects. We also note a systematic offset of $+0.08$ dex between [Ti I/Fe I] and [Ti II/Fe II], especially for RGB stars. However, taking into account that the oscillator strength values

of the Ti II lines are highly uncertain and that the offset is still reasonably small, we can conclude that the [X/Fe] abundance ratio can be safely constrained either by neutral or by single-ionized lines. It is also interesting to note that the average [Ti I/Fe] and [Ti II/Fe] abundance ratios ($+0.16$ dex and $+0.25$ dex, respectively) of Yong et al. (2014) show a relative offset of -0.09 dex, which is similar to ours but in the opposite direction. This suggests that there is an intrinsic (although small) uncertainty in the zero-point scale of the titanium abundance.

AGB star 96: As apparent from Figure 3, AGB star 96 shows a difference between neutral and ionized abundances, both for iron and titanium, which is incompatible with those found for the other AGB targets, and which is much more similar to the values measured for RGB stars. Interestingly, star 96 presents atmospheric parameters compatible with those spanned by the RGB targets (but with a surface gravity that is 0.15–0.2 lower than that of RGB stars at the same temperature). This case is
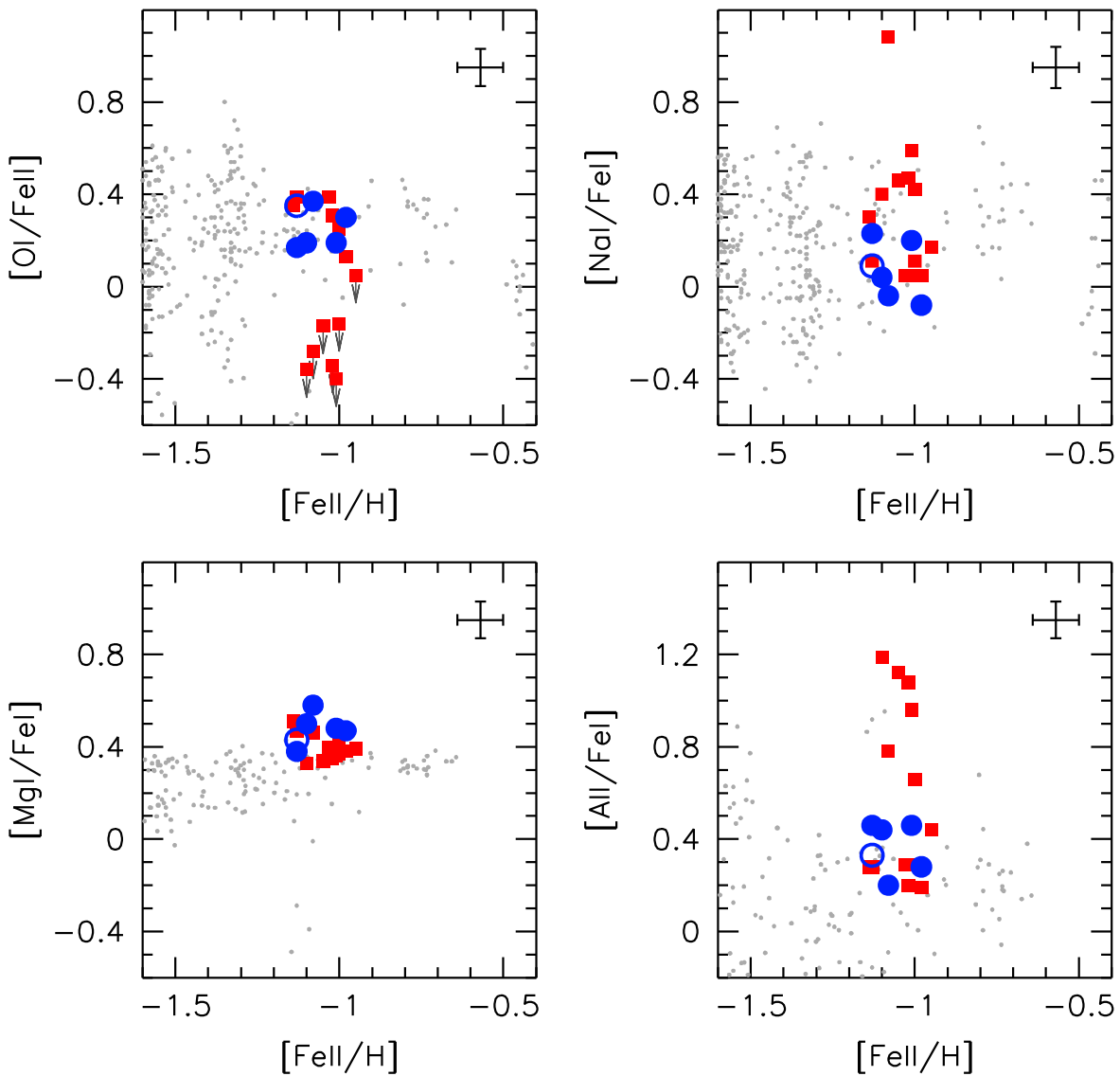
Figure 5. From top left to bottom right, oxygen, sodium, magnesium, and aluminum abundance ratios as a function of [Fe II/H] for the studied sample of stars (same symbols as in Figure 1). For a subsample of (O-poor) RGB stars, only upper limits to the oxygen abundance could be measured from the acquired spectra (see arrows). Representative error bars are marked in the top right corner of each panel. The values measured in large samples of giant stars in 20 Galactic GCs (from GIRAFFE and UVES spectra by Carretta et al. 2009b, 2009c, 2014), rescaled to the solar values adopted in this work, are shown for reference as gray dots.

similar to that encountered in 47Tuc, where the Fe I abundance of a small subsample of AGB stars (four out of 24) has been found to agree with the value obtained from ionized lines, thus suggesting that one of the possible explanations could be the lack of LTE departures for these objects (Lapenna et al. 2014). Also in M22, one (out of five) AGB star shows a perfect agreement between [Fe I/H] and [Fe II/H], whereas the other AGB stars show systematically low [Fe I/H] values (Mucciarelli et al. 2015b).

3.2. Oxygen, Sodium, Magnesium, and Aluminum

In most Galactic GCs, the abundances of oxygen, sodium, magnesium, and aluminum are known to show large star-to-star variations, organized in clear correlations (see Gratton et al. 2012 for a review). These are usually interpreted as the signature of self-enrichment processes occurring in the early stages of GC evolution and giving rise to at least two stellar generations with a very small (if any) age difference,

commonly labeled as first and second generations (FG and SG, respectively). In particular, the variations observed in O, Na, Mg, and Al are thought to be due to the ejecta from still unclear polluters, like massive AGB stars, fast-rotating massive stars, or massive binaries (Fenner et al. 2004; Ventura & D'Antona 2005; Decressin et al. 2007; de Mink et al. 2009; Marcolini et al. 2009; Bastian et al. 2013, 2015).

To also verify the presence of these key features in our sample of giants, we derived the abundances of O, Na, Al, and Mg from the observed spectra. The results are shown in Figure 5, where all abundance ratios are plotted as a function of the iron content as measured from the ionized lines. Since the oxygen abundance derived from the forbidden [O I] line at 6300.3 Å is not affected by NLTE, its abundance ratio is expressed with respect to the "true" iron content (measured from Fe II lines). Instead, the other species are known to suffer from NLTE effects, and their abundances are therefore plotted with respect to Fe I (see Section 3.1). This is true also for
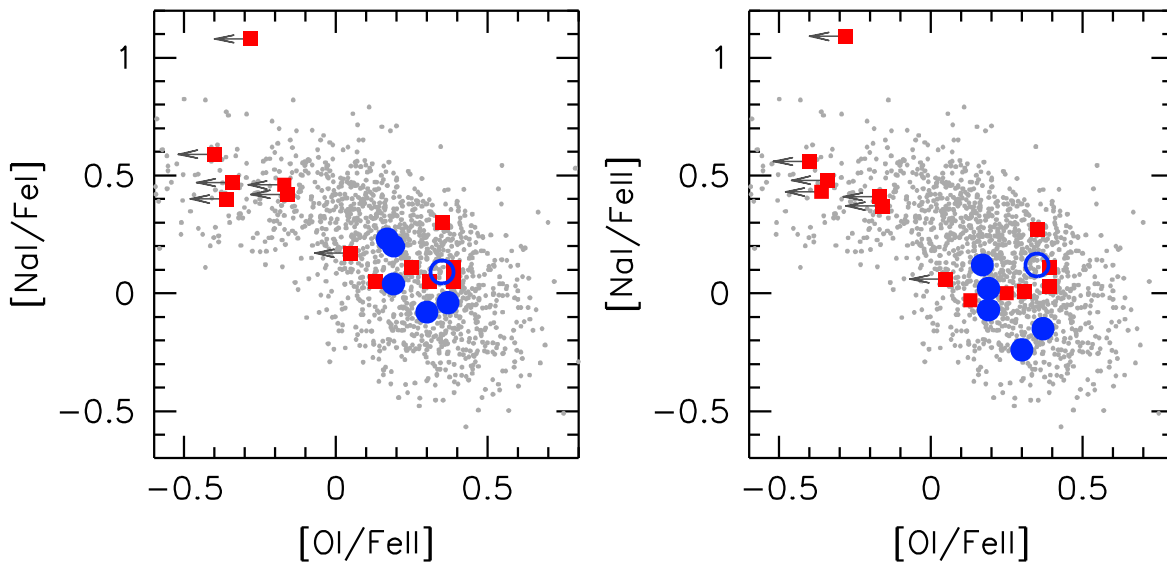
Figure 6. Oxygen–sodium anticorrelation measured for the observed stars (same symbols as in Figure 5). The corrections for NLTE effects provided by Gratton et al. (1999) have been applied to the Na abundances. This is then expressed with respect to Fe I and to Fe II in the left and right panels, respectively. Gray dots are as in Figure 5.
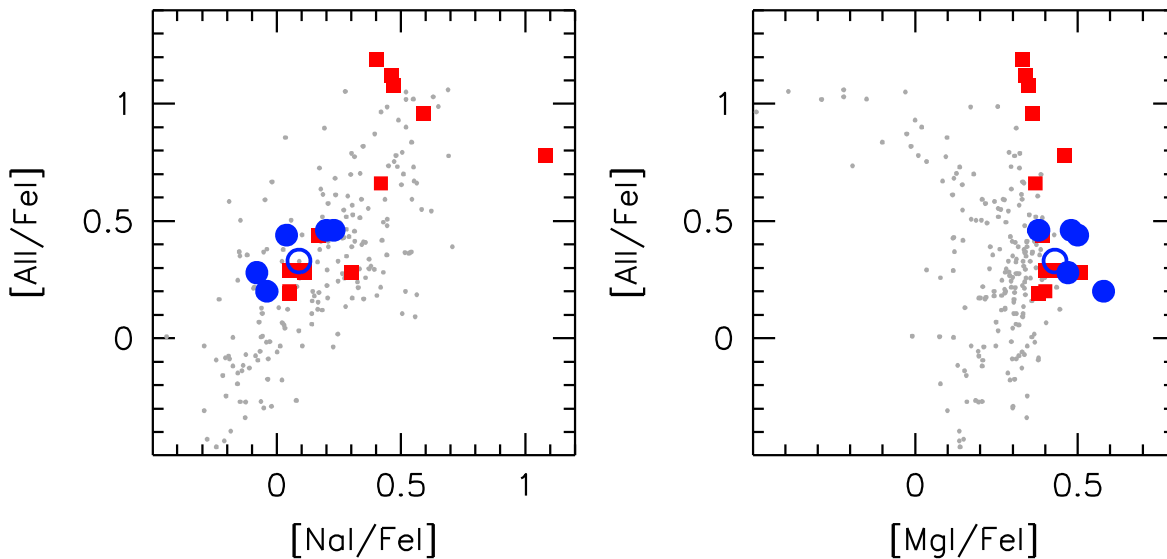

Figure 7. Aluminum–sodium correlation (left panel) and aluminum–magnesium anticorrelation (right panel) for the observed stars (same symbols as in Figure 5). Gray dots as in Figure 5.

sodium, although we have applied the NLTE corrections of Gratton et al. (1999), which take into account departures from LTE conditions driven by overrecombination (Bergemann & Nordlander 2014).[11] In any case, we have verified that the same results are obtained if the Na, Al, and Mg abundances are computed with respect to Fe II or H. In agreement with what is commonly observed in Galactic GCs, we find that the Mg abundance is constant within the uncertainties, whereas O, Na, and Al show significant (several tenths of a dex) star-to-star variations in the RGB sample (see also Yong et al. 2014). As shown in Figures 6 and 7, the observed star-to-star variations are organized in the same correlations observed for GCs. In particular, oxygen and sodium are anticorrelated, independently of using Fe I or Fe II for the computation of the sodium

abundance ratio (Figure 6), whereas aluminum and sodium are positively correlated, and [Al I/Fe I] shows a ∼1 dex spread for fixed magnesium (Figure 7). Very interestingly, instead, all abundance ratios are constant for the AGB sample, with values mainly consistent with those commonly associated with the FG.

The Na–O anticorrelation derived from our RGB sample is qualitatively compatible with that measured by Yong et al. (2014), who found two groups of stars well separated both in [Na/Fe] and [O/Fe]. We note that the oxygen abundances quoted by Yong et al. (2014) are larger than ours, with an average offset of +0.5 dex for the O-rich stars. The origin of this discrepancy can be ascribable to different factors (like atomic data, telluric correction, and so on), but it is beyond the aims of this paper. A good agreement with the results of Yong et al. (2014) is found also for the [Al/Fe] and [Mg/Fe] distributions.

---

[11] By adopting the NLTE corrections of Lind et al. (2011), the differential behavior between AGB and RGB stars remains the same.
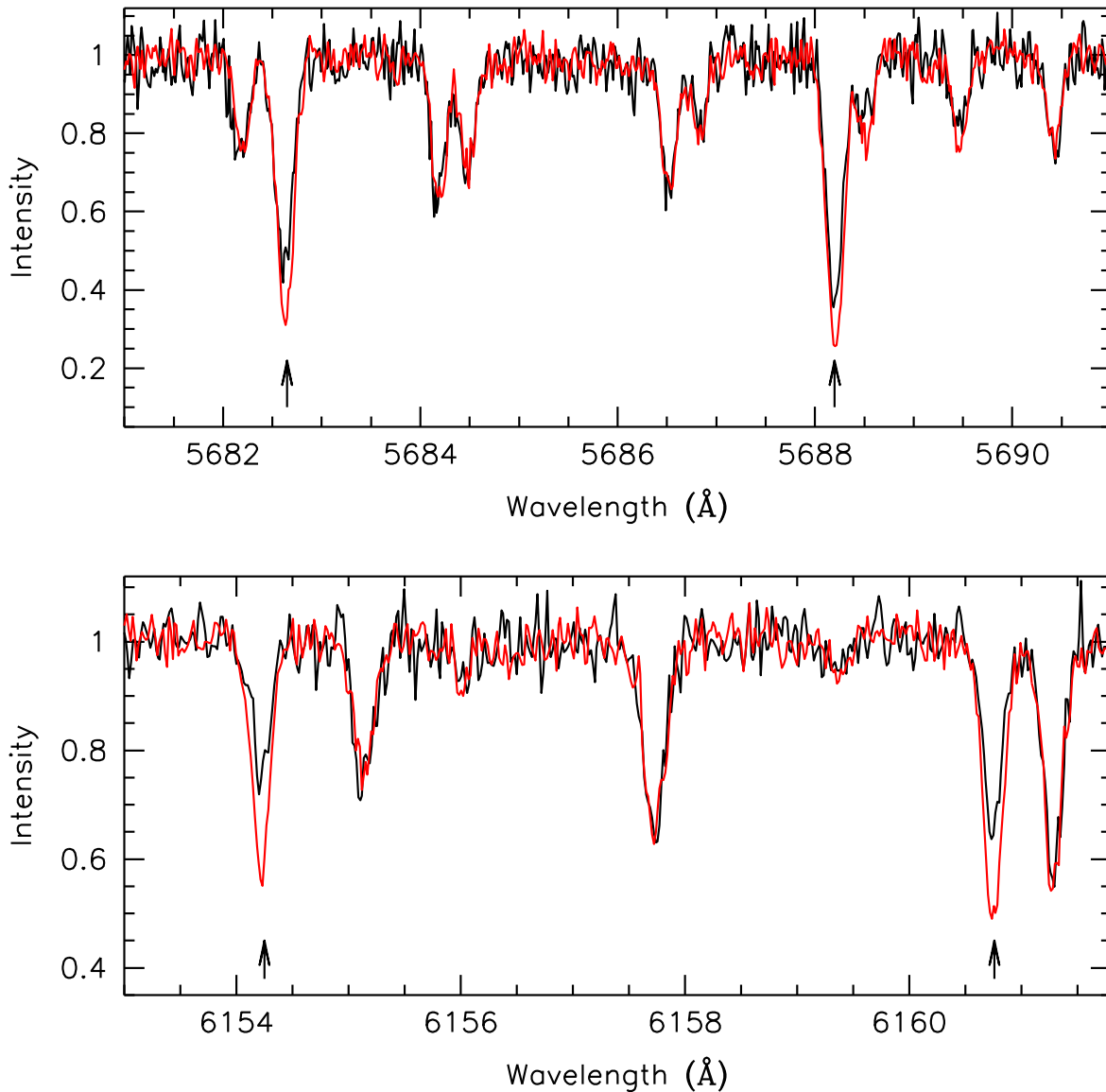
Figure 8. Comparison between the spectra of the RGB stars 89 (red line) and 95 (black line) for the NaI lines at 5682–5688 Å (top panel) and 6154–6160 Å (bottom panel). The black arrows mark the position of the Na lines.

The derived Na–O anticorrelation of M62 is more extended than those observed in most Galactic GCs. Two discrete groups of stars can be recognized, a first one with [O/Fe] $\sim$ +0.2/ +0.3 dex and [Na/Fe] $\sim$ +0.1 dex, and a second group with [O/Fe] < 0.0 dex (only upper limits) and [Na/Fe] at $\sim$+0.5 dex. In particular, the subsolar O-poor component (the so-called "extreme population"; see Carretta et al. 2010a) is quite prominent in M62, although these stars are usually rare, observed only in some massive systems, such as NGC 2808 (Carretta et al. 2009c), M54 (Carretta et al. 2010b), and ω Centauri (Johnson & Pilachowski 2010). We also find a significant lack of "intermediate population" stars (with enhanced Na abundances and mild oxygen depletion (Carretta et al. 2010a), which are instead the dominant component in most GCs.

We finally note that the RGB star 89 exhibits a Na abundance of [Na/Fe] = +1.08 dex, which is $\sim$0.5 dex larger than that measured for all the other O-poor stars. In Figure 8 we compare the spectrum of star 89 with that of another RGB

target (id = 95) having very similar atmospheric parameters and iron abundances (see Table 3). As is apparent, all lines have the same strengths, with the notable exception of the two Na doublets, which are significantly stronger in star 89.

To our knowledge, this is one of the most Na-rich giants ever detected in a genuine GC (see also the comparison with literature data in Figure 6), with a [Na/Fe] abundance even higher than the most Na-rich stars observed in NGC 2808 (Carretta et al. 2006) and NGC 4833 (Carretta et al. 2014), and comparable to a few extremely Na-rich objects observed in the multi-iron system ω Centauri (Marino et al. 2011).

4. DISCUSSION AND CONCLUSIONS

The differences in the iron and titanium abundances measured from neutral and from single-ionized lines in five AGB stars of M62 closely resemble those found in M5 (Ivans et al. 2001), 47Tuc (Lapenna et al. 2014), and NGC 3201 (Mucciarelli et al. 2015a). These results might be explained as the consequences of departures from LTE conditions, affecting

the neutral species, while leaving unaltered the ionized lines. The final effect is a systematic underestimate of the chemical abundances if measured from neutral features. Interestingly, the findings in M5, 47Tuc, and NGC 3201 seem to suggest that this effect concerns most, but not all, AGB stars, while it is essentially negligible for RGB targets. This is inconsistent with the available NLTE calculations (e.g., Bergemann et al. 2012; Lind et al. 2012), which predict the same corrections for stars with similar parameters. Moreover, the results recently obtained in M22 show that the situation is even more complex. In M22, in fact, neutral iron abundances systematically lower than [Fe II/H] have also been measured for RGB stars (Mucciarelli et al. 2015b). However, the [Fe I/H]–[Fe II/H] difference in M22 clearly correlates with the abundance of s-process elements (that show intrinsic star-to-star variations unusual for GCs), suggesting that this could be a distinct, peculiar case. All these results seem to suggest that we are still missing some crucial detail about the behavior of chemical abundances in the case of departures from LTE conditions, or that other ingredients (such as full three-dimensional, spherical hydro calculations, and the inclusion of chromospheric components) should be properly taken into account in modeling the atmospheres of these stars.

For all the studied stars we have also determined the abundances of O, Na, Mg, and Al from the neutral lines available. As shown in Figures 6 and 7, our sample of RGB stars shows the typical behaviors observed in all massive GCs, with large and mutually correlated dispersions of O, Na, and Al (and with one of the most Na-rich giants ever observed in a GC: RGB star 89, with [Na/Fe] = +1.08 dex). Instead, the light-element abundances of AGB stars are essentially constant and clumped at the low end of the Na and Al values of the RGB sample.

If the (still unclear) NLTE effects impacting the Fe I and Ti I abundances of the AGB targets significantly weaken the minority species lines (as it seems reasonable to assume), the measured abundances of sodium, aluminum, and magnesium could also be underestimated for these objects (even when referred to the neutral iron abundance, Fe I). Thus, although the observed star-to-star variation of Na in most GCs is often a factor of 5–10 larger than the suspected NLTE effects on Fe and Ti, we caution that it could be risky to derive firm conclusions about a lack of Na-rich AGB stars on the basis of the sodium abundance alone until these effects are properly understood and quantified (of course, the same holds for any other light element potentially affected by NLTE effects, especially if the star-to-star variations of this element are intrinsically small). In fact, a lack of Na-rich AGB stars could be either real or just due to a bias induced by NLTE effects. Solid evidence, instead, is obtained if the result is based on elemental species (like the oxygen abundance derived from the forbidden line considered here) that are virtually unaffected by NLTE effects. Hence, Figure 6, showing that the oxygen abundances of all AGB stars are larger than those expected for the SG population and measured, in fact, for a subsample of RGB giants, convincingly indicates that none of the AGB targets studied in M62 is compatible with the SG of the cluster.

Does this mean that the SG stars in M62 did not experience the AGB phase (as has been suggested for NGC 6752 by Campbell et al. 2013)? To answer this question we note that, although variable from cluster to cluster, the typical percentages of FG and SG stars in Galactic GCs are 30% and 70%,

respectively (e.g., Carretta 2013; Bastian & Lardo 2015). On this basis, we should have observed four second-generation AGB stars in our sample. Alternatively, based on Figures 6 and 7 we see that six out of 13 (46%) RGB stars likely belong to the SG, and we could have therefore expected two to three AGB stars in the same group, at odds with what is observed. On the other hand, a deficiency of CN-strong (second-generation) AGB stars in several GCs has been known since the pioneering work of Norris et al. (1981), and it has been recently found to be most severe in GCs with the bluest HB morphology (see, e.g., Gratton et al. 2010, and references therein). While M62 has indeed a very extended HB, it shows no deficiency of AGB stars. In fact, by using ACS and WFC3 *HST* archive data acquired in the m_{F390W} and m_{F658N} filters, we counted the number of AGB and HB stars (86 and 640, respectively) in M62, finding that their ratio (the so-called R_2 parameter; Caputo et al. 1989) is $R_2 \simeq 0.13$. This value is in very good agreement with the theoretical predictions based on the ratio between the AGB and the HB evolutionary timescales (e.g., Cassisi et al. 2001). Hence, our observations show that all of the sampled AGB stars belong to the FG, but we cannot exclude that some SG object is present along the AGB of M62.

Clearly, if a complete lack of SG AGB stars is confirmed by future studies in M62, NGC 6752, M13 (see, e.g., Sneden et al. 2000; Johnson & Pilachowski 2012), or any other GC, this will represent a new challenge for the formation and evolution models of these stellar systems (as already discussed, e.g., by Charbonnel et al. 2013 and Cassisi et al. 2014).

REFERENCES

Alonso, A., Arribas, S., & Martínez-Roger, C. 1999, A&AS, 140, 261
Bastian, N., Cabrera-Ziri, I., & Salaris, M. 2015, MNRAS, 449, 3333
Bastian, N., Lamers, H. J. G. L. M., de Mink, S. E., et al. 2013, MNRAS, 436, 2398
Bastian, N., & Lardo, C. 2015, MNRAS, 453, 357
Beccari, G., Ferraro, F. R., Possenti, A., et al. 2006, AJ, 131, 2551
Bergemann, M., Lind, K., Collet, R., Magic, Z., & Asplund, M. 2012, MNRAS, 427, 27
Bergemann, M., & Nordlander, T. 2014, arXiv:1403.3088
Bertaux, J. L., Lallement, R., Ferron, S., Boonne, C., & Bodichon, R. 2014, A&A, 564, A46
Bressan, A., Marigo, P., Girardi, L., et al. 2012, MNRAS, 427, 127
Briley, M. M., Smith, G. H., Hesser, J. E., & Bell, R. A. 1993, AJ, 106, 142
Caffau, E., Ludwig, H.-G., Steffen, M., Freytag, B., & Bonifacio, P. 2011, SoPh, 268, 255
Campbell, S. W., D'Orazi, V., Yong, D., et al. 2013, Natur, 498, 198
Caputo, F., Chieffi, A., Tornambe, A., Castellani, V., & Pulone, L. 1989, ApJ, 340, 241
Carretta, E. 2013, A&A, 557, A128
Carretta, E., Bragaglia, A., Gratton, R., D'Orazi, V., & Lucatello, S. 2009a, A&A, 508, 695
Carretta, E., Bragaglia, A., Gratton, R., & Lucatello, S. 2009b, A&A, 505, 139
Carretta, E., Bragaglia, A., Gratton, R. G., et al. 2006, A&A, 450, 523
Carretta, E., Bragaglia, A., Gratton, R. G., et al. 2009c, A&A, 505, 117
Carretta, E., Bragaglia, A., Gratton, R. G., et al. 2010a, A&A, 516, 55
Carretta, E., Bragaglia, A., Gratton, R. G., et al. 2010b, A&A, 514, 7
Carretta, E., Bragaglia, A., Gratton, R. G., et al. 2014, A&A, 564, A60
Cassisi, S., Castellani, V., Degl'Innocenti, S., Piotto, G., & Salaris, M. 2001, A&A, 366, 578

Cassisi, S., Salaris, M., Pietrinferni, A., Vink, J. S., & Monelli, M. 2014, A&A, 571, A81

Charbonnel, C., Chantereau, W., Decressin, T., Meynet, G., & Schaerer, D. 2013, A&A, 557, L17

Cioni, M.-R. L., & Habing, H. J. 2003, A&A, 402, 133

D'Amico, N., Lyne, A. G., Manchester, R. N., Possenti, A., & Camilo, F. 2001, ApJL, 548, L171

de Mink, S. E., Pols, O. R., Langer, N., & Izzard, R. G. 2009, A&A, 507, L1

Decressin, T., Meynet, G., Charbonnel, C., Prantzos, N., & Ekström, S. 2007, A&A, 464, 1029

D'Ercole, A., Vesperini, E., D'Antona, F., McMillan, S. L. W., & Recchi, S. 2008, MNRAS, 391, 825

Dubath, P., Meylan, G., & Mayor, M. 1997, A&A, 324, 505

Fenner, Y., Campbell, S., Karakas, A. I., Lattanzio, J. C., & Gibson, B. K. 2004, MNRAS, 353, 789

Ferraro, F. R., Fusi Pecci, F., Testa, V., et al. 1995, MNRAS, 272, 391

Fuhr, J. R., Martin, G. A., & Wiese, W. L. 1988, in Journal of Physical and Chemical Reference Data, Vol. 17 (New York: AIP), 4

Fuhr, J. R., & Wiese, W. L. 2006, JPCRD, 35, 1669

Gratton, R. G., Carretta, E., & Bragaglia, A. 2012, A&ARv, 20, 50

Gratton, R. G., Carretta, E., Bragaglia, A., Lucatello, S., & D'Orazi, V. 2010, A&A, 517, A81

Gratton, R. G., Carretta, E., Eriksson, K., & Gustafsson, B. 1999, A&A, 350, 955

Gratton, R. G., Sneden, C., Carretta, E., & Bragaglia, A. 2000, A&A, 354, 169

Grevesse, N., & Sauval, A. J. 1998, SSRv, 85, 161

Harris, W. E. 1996, AJ, 112, 1487

Hill, V., Lecureur, A., Gómez, A., et al. 2011, A&A, 534, A80

Hoefner, S., Jorgensen, U. G., Loidl, R., & Aringer, B. 1998, A&A, 340, 497

Ivans, I. I., Kraft, R. P., Sneden, C., et al. 2001, AJ, 122, 1438

Ivans, I. I., Sneden, C., Kraft, R. P., et al. 1999, AJ, 118, 1273

Johnson, C. I., McDonald, I., Pilachowski, C. A., et al. 2014, AJ, 149, 71

Johnson, C. I., McWilliam, A., & Rich, R. M. 2013, ApJL, 775, L27

Johnson, C. I., & Pilachowski, C. A. 2010, ApJ, 722, 1373

Johnson, C. I., & Pilachowski, C. A. 2012, ApJL, 754, L38

Kraft, R. P., & Ivans, I. I. 2003, PASP, 115, 143

Lapenna, E., Mucciarelli, A., Lanzoni, B., et al. 2014, ApJ, 797, 124

Lawler, J. E., Guzman, A., Wood, M. P., Sneden, C., & Cowan, J. J. 2013, ApJS, 205, 11

Lind, K., Asplund, M., Barklem, P. S., & Belyaev, A. K. 2011, A&A, 528, A103

Lind, K., Bergemann, M., & Asplund, M. 2012, MNRAS, 427, 50

Mallia, E. A. 1978, ApJ, 104, 645

Maraston, C. 2005, MNRAS, 362, 799

Marcolini, A., Gibson, B. K., Karakas, A. I., & Sánchez-Blázquez, P. 2009, MNRAS, 395, 719

Marino, A. F., Milone, A. P., Piotto, G., et al. 2011, ApJ, 731, 64

Martin, G. A., Fuhr, J. R., & Wiese, W. L. 1988, Atomic transition probabilities. Scandium through Manganese (New York: AIP and American Chemical Society)

Mashonkina, L., Gehren, T., Shi, J.-R., Korn, A. J., & Grupp, F. 2011, A&A, 528, A87

Massari, D., Mucciarelli, A., Dalessandro, E., et al. 2012, ApJL, 755, L32

McCall, M. L. 2004, AJ, 128, 2144

Mucciarelli, A. 2013a, arXiv:1311.1403

Mucciarelli, A., Lapenna, E., Massari, D., Ferraro, F. R., & Lanzoni, B. 2015a, ApJ, 801, 69

Mucciarelli, A., Lapenna, E., Massari, D., et al. 2015b, ApJ, 809, 128

Mucciarelli, A., Origlia, L., Ferraro, F. R., Maraston, C., & Testa, V. 2006, ApJ, 646, 939

Mucciarelli, A., Origlia, L., Ferraro, F. R., & Pancino, E. 2009, ApJL, 695, L134

Mucciarelli, A., Pancino, E., Lovisi, L., Ferraro, F. R., & Lapenna, E. 2013b, ApJ, 766, 78

Neckel, H., & Labs, D. 1984, SoPh, 90, 205

Ness, M., Freeman, K., Athanassoula, E., et al. 2013, MNRAS, 430, 836

Norris, J., Cottrell, P. L., Freeman, K. C., & Da Costa, G. S. 1981, ApJ, 244, 205

O'Brian, T. R., Wickliffe, M. E., Lawler, J. E., Whaling, W., & Brault, J. W. 1991, JOSAB, 8, 1185

Pasquini, L., Avila, G., Allaert, E., et al. 2000, Proc. SPIE, 4008, 129

Pooley, D., Lewin, W. H. G., Anderson, S. F., et al. 2003, ApJL, 591, L131

Raassen, A. J. J., & Uylings, P. H. M. 1998, A&A, 340, 300

Renzini, A., & Buzzoni, A. 1986, Spectral Evolution of Galaxies, 122 (Dordrecht: Reidel), 195

Robin, A. C., Reylé, C., Derrière, S., & Picaud, S. 2003, A&A, 409, 523

Sbordone, L. 2005, MSAIS, 8, 61

Sneden, C., Ivans, I. I., & Kraft, R. P. 2000, MmSAI, 71, 657

Stetson, P. B., & Pancino, E. 2008, PASP, 120, 1332

Storey, P. J., & Zeippen, C. J. 2000, MNRAS, 312, 813

Thévenin, F., & Idiart, T. P. 1999, ApJ, 521, 753

van Loon, J. T., Groenewegen, M. A. T., de Koter, A., et al. 1999, A&A, 351, 559

Ventura, P., & D'Antona, F. 2005, ApJL, 635, L149

Wolnik, S. J., & Berthel, R. O. 1973, ApJ, 179, 665

Wood, M. P., Lawler, J. E., Sneden, C., & Cowan, J. J. 2013, ApJS, 208, 27

Worley, C. C., Cottrell, P. L., Freeman, K. C., & Wylie-de Boer, E. C. 2009, MNRAS, 400, 1039

Yong, D., Alves Brito, A., Da Costa, G. S., et al. 2014, MNRAS, 439, 2638

Zoccali, M., Hill, V., Lecureur, A., et al. 2008, A&A, 486, 177